ACS APPLIED MATERIALS & INTERFACES

Research Article

www.acsami.org

Kinetics and Interfacial Thermodynamics of the pH-Related Sorption of Tetrabromobisphenol A onto Multiwalled Carbon Nanotubes

Yunhai Zhang, Guicai Liu, Shuili Yu,* Jun Zhang, Yulin Tang,* Pan Li, and Yifei Ren

State Key Laboratory of Pollution Control and Resource Reuse, College of Environmental Science & Engineering, Tongji University, Shanghai 200092, China

Supporting Information

ABSTRACT: Surface functionalization of multiwalled carbon nanotubes (MWCNTs) was performed using mixed acid and ethylenediamine. The materials were characterized by electron microscope, X-ray diffraction, Raman spectra, Fourier transform infrared, N_2 adsorption−desorption, and X-ray photoelectron spectroscopy. The pH-dependent sorption of tetrabromobisphenol A (TBBPA) onto raw and functionalized MWCNTs was investigated. A decrease in TBBPA uptake was found to be dependent on the adsorptive pK_a in alkaline conditions. Two types of MWCNTs exhibited rapid binding kinetics for TBBPA sorption within 20 min. The kinetics of TBBPA sorption onto MWCNTs were analyzed using a pseudo-second-order model, an intraparticle diffusion model and Boyd model. The results showed that TBBPA sorption on MWCNTs and N-MWCNTs could be well described by the pseudo-second-order model, and the external diffusion (boundary layer diffusion) was the rate-limiting step. The extended Derjaguin−Landau−Verwey−Overbeek (XDLVO) theory was applied to calculate interfacial free energies and to explain the sorption characteristics between the sorbent and solute. This analysis revealed that hydrophobic attractive interactions (i.e., interfacial AB interactions) were dominant in TBBPA sorption onto MWCNTs.

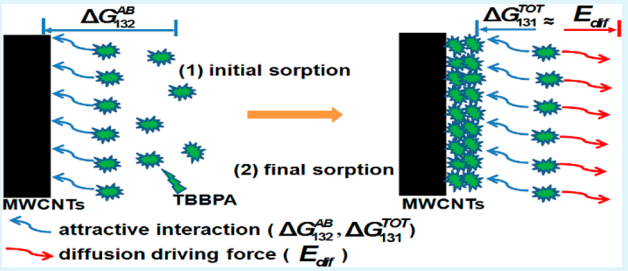

KEYWORDS: *sorption, kinetics, XDLVO, tetrabromobisphenol A, MWCNTs*

1. INTRODUCTION

Tetrabromobisphenol A (TBBPA) has attracted great concern as an environmental threat because of its global distribution and bioaccumulation. TBBPA has been found in soil,[1] aquatic sediment,[2] wastewater,[3] source water,[4−6] and even in the indoor environment.[7] It has also been detected in human plasma serum and in the breast milk of women throughout the world.[7−9] This compound is considered a potential endocrine disruptor because of its structural resemblance to the thyroid hormone thyroxin. The effect of TBBPA on humans, notably in pregnant women and neonates, has attracted much attention.[10] The high maternal transferability of TBBPA transfer might lead to the strong accumulation of TBBPA in the infant.[11] Therefore, a feasible means of eliminating TBBPA contamination must be found.

Several methods for TBBPA removal, such as sorption,[12,13] oxidation,[14,15] photocatalysis,[16,17] and biological degradation,[18] have been reported in recent decades. Among these methods, sorption has been considered as a simple and highly efficient technique for TBBPA removal from water. CNTs have attracted widespread attention as a new type of adsorbent for the removal of various inorganic and organic pollutants. CNTs are advantageous because of their large surface areas and significant $\pi-\pi$ electrostatic interactions.[12,13,19−21] To date, few studies have reported the sorption behavior of TBBPA onto pure MWCNTs[12] and magnetic nanocomposites.[13] However, because TBBPA is a hydrophobic substance, to increase the solubility of TBBPA, researchers have added a certain amount of organic solvent, such as methanol, to study the sorption.[13,22,23] This procedure inevitably generates a solvent effect, seriously affecting the sorption characteristics.[22,23] To avoid cosolvent effects and remove TBBPA in as close to real-world water environments, the volume fraction of methanol in the sorption solution was kept at less than 0.1% in our study.

The main adsorption interactions of phenolic organic compounds onto CNTs include hydrophobic effects, π-electron donor−acceptor bonds, and hydrogen bonds.[24−27] Moreover, van der Waals forces may be significant for adsorption from the aqueous phase.[27] Pan et al. indicated that the $\pi-\pi$ electron donor−acceptor system is the predominant mechanism involved in the adsorption of BPA onto CNMs according to a comparison of K_{HW} normalized adsorption coefficients.[28] Li et al. considered that the adsorption of weak acids onto CNTs was facilitated by the formation of a negative charge-assisted H-bond (−) CAHB between the weak acids and the O-rich CNTs.[27] However, the role and the contribution rate of the hydrophobic effect and van der Waals force mechanism in the sorption process have rarely been reported. The sorption of organic matter by CNTs is generally pH-dependent because solution pH not only influences the properties of the adsorbent

Received: August 25, 2014
Accepted: November 17, 2014
Published: November 17, 2014

surface but also affects the speciation of target pollutants in solution.[24,29,30] In the present study, we focus on the sorption of the weak acid TBBPA onto CNTs. The extended Derjaguin−Landau−Verwey−Overbeek (XDLVO) theory was proposed based on a detailed study of three major interfacial interactions of the Lewis acid−base (AB), Lifshitz−van der Waals (LW), and electrostatic double layer (EL) interactions, LW and EL are the basic interactions in DLVO theory.[31−33] The LW and AB interactions were predominantly investigated in this study for TBBPA sorption onto CNTs.

The sorption characteristics of the interactions between MWCNTs and TBBPA in water were studied kinetically using a pseudo-second-order model, an intraparticle diffusion model and Boyd model. A series of experiments were designed to reveal the mechanisms involved in TBBPA sorption onto MWCNTs. Additionally, the interactions were monitored by quantitatively measuring the interfacial free energies of TBBPA−MWCNTs adhesion and TBBPA−TBBPA cohesion. Applications of XDLVO in membrane fouling were transplanted into sorption in aqueous solution to elucidate the interaction forces between contaminants and adsorbent. This process can provide a guide to a range of practical applications of adsorbents to remove contaminants in water treatment.

2. EXPERIMENTAL SECTION

2.1. Materials and Reagents. Both 4,4-isopropylidenebis (2,6-dibromophenol) (TBBPA, >97%) and methanol (HPLC grade) were obtained from Sigma-Aldrich Company (MO, USA). Ethylenediamine (EDA) and *n*,*n*-dicyclohexylcarbodiimide (DCC, 99%) were purchased from the Aladdin Company (Shanghai, China). All other chemicals used in this study were guaranteed reagent grade and purchased from Sinopharm Chemical Reagents (Shanghai, China). Ultrapure water with a resistivity of 18.2 MΩ·cm was obtained from a Milli-Q Integral 15 system (Millipore, MA, USA). MWCNTs were obtained from Seldon Technologies (VT, USA, >97%) with nominal outer diameters of 10−20 nm and inner diameters of 5−10 nm. The preparation of functionalized MWCNTs was analogous to that reported in the literature.[34,35] Details of the surface modification of MWCNTs are provided in the Supporting Information.

2.2. Instrumentation and Analytical Method. The microstructure and morphology of the raw and modified MWCNTs were characterized using scanning electron microscopy (SEM, Philips XL30, Netherland), transmission electron microscopy (TEM, JEOL 2011, Japan), X-ray diffractometry (XRD, D8 Advance, Bruker, Germany) and Raman spectroscopy (LabRam-1B, JY, France). The specific surface area and pore size distribution of the adsorbents were calculated from the adsorption−desorption isotherms of N_2 at 77 K by the multipoint BET method and BJH method on an ASAP 2010 micropore physisorption analyzer (Micromeritics, GA, USA). The surface functional groups of raw and modified MWCNTs were detected with a Fourier Transform Infrared Ray (FT-IR) Spectrometer (NICOLET 5700, PerkinElmer, MA, USA) from 4000 to 500 cm^{-1}. X-ray photoelectron spectroscopic (XPS) analyses are performed with a Kratos Axis Ultra DLD Spectrometer at a base pressure of 1×10^{-9} Torr (Shimadzu, Japan). The pH values of the supernatants were measured using an S20 SevenEasy pH meter (Mettler-Toledo, Shanghai, China). The zeta potential was determined with a zeta potential analyzer (Zetasizer Nano Z, Malvern Instrument, Worcestershire, UK).

The contact angles were measured using a JC2000D contact angle goniometer (Zhongchen Digital Technology Apparatus, Shanghai, China). At least ten equilibrium contact angles were measured for each material. The highest and lowest values were discarded before taking the average and standard deviation. The probe liquids selected for this investigation were diiodomethane, formamide, ultrapure water, and aqueous solutions at different pH.

Concentrations of TBBPA were determined using ultraperformance liquid chromatography (UPLC; with a TUV detector, ACQUITY UPLC H-Class, Waters, MA, USA) with a reversed phase BEH C18 Column (2.1 × 50 mm, 1.7 μm). TBBPA was measured in an isocratic elution program with methanol/water (75:25, v/v) as the mobile phase. The flow rate was maintained at 0.2 mL/min, and the injection volume was 5 μL. The detection wavelength was 209 nm, and the temperature of the column was 303 K.

2.3. Batch Sorption Experiment. Batch experiments were employed to evaluate characteristics of and mechanism involved in TBBPA sorption onto MWCNTs. Typically, prior to starting the sorption experiment, 250 mL of the TBBPA solution (at an initial concentration of approximately 2.0 mg/L) was transferred to a 250 mL Erlenmeyer flask. The background solution was 0.01 M NaCl to maintain a stable ionic strength. A measured amount of MWCNTs was prewetted and then ultrasonically dispersed for 20 min. Afterward, 200 μL of the MWCNT stock solution (10 mg/mL) was injected into the solution with a micropipette. The volume fraction of methanol in the sorption solution was maintained at less than 0.1% to avoid cosolvent effects. When necessary, 0.1 M HCl and 0.1 M NaOH solutions were used to adjust the solution pH. The pH effect on the sorption of TBBPA on MWCNTs was investigated in a pH range from 7.0 to 10.0 (±0.3). The bottles containing a mixture of TBBPA and MWCNTs were transferred to a thermostatic air shaker under 180 rpm at 303 K. At designated time intervals (2, 3, 4, 5, 8, 15, 30, 60, 90, 120, and 360 min), 1.0 mL of the mixture solution was withdrawn from the vial and centrifuged at 12 000 rpm for 5 min and the supernatants were analyzed by UPLC to determine the residual concentrations of TBBPA. The average values of all sorption experiments performed in triplicates were reported and the standard errors for the duplicates were usually less than 5%. The TBBPA uptake on MWCNTs can be calculated by eq 1

$$q_t = \frac{(C_0 - C_t)V}{m} \tag{1}$$

where q_t (mg/g) is the sorbed amount of TBBPA, C_0 and C_t (mg/L) are the concentration at initial and at time t (min), respectively, V (L) is the volume of solution, and m (g) is the mass of MWCNTs.

2.4. Kinetic Models. Determining the sorption kinetic behavior for TBBPA on MWCNTs is important in understanding the rate processes occurring in aqueous solution. These processes may help explain the mechanism of sorption along with the reaction pathways. In this Research Article, the experimental data were fitted by a pseudo-second-order model, an intraparticle diffusion and Boyd kinetic model. For the pseudo-second-order kinetics model, the sorption process can be described as in eq 2

$$\frac{t}{q_t} = \frac{1}{k_2 q_e^{\,2}} + \frac{1}{q_e} e \tag{2}$$

where q_e is the sorption amount (mg/g) at equilibrium, q_t is the sorption amount (mg/g) at time t (min), and k_2 is the pseudo-second-order rate constant; the initial sorption rate h (mg/g min) can be determined from $h = K_2 q_e^{\,2}$.

For the intraparticle diffusion model,[36] the sorption process can be described as in eq 3

$$q_t = k_{id} t^{1/2} + C \tag{3}$$

where k_{id} is the intraparticle diffusion rate constant (mg/g $min^{1/2}$) and C (mg/g) is a constant proportional to the thickness of the boundary layer.

The sorption kinetic data was further analyzed by Boyd kinetic model,[37,38] which can be calculated by eq 4

$$Bt = -\ln\left(1 - \frac{q_t}{q_e}\right) - 0.4977 \tag{4}$$

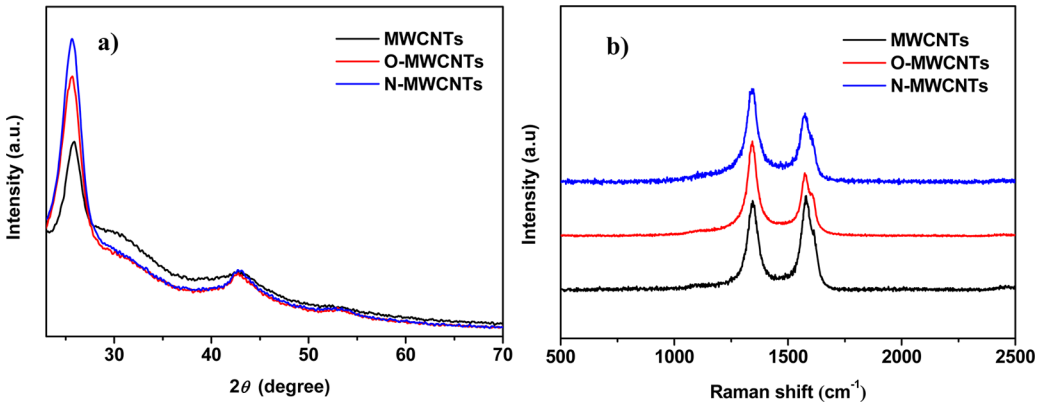

Figure 1. (a) XRD patterns and (b) Raman spectra of MWCNTs, O-MWCNTs, and N-MWCNTs.

where $B = \pi^2 D_i/r^2$, D_i is the effective diffusion coefficient, and r is the particle radius calculated by sieve analysis and assuming spherical particles.

The average sorption rate was introduced between TBBPA-MWCNTs and between the TBBPAs themselves for the interfacial thermodynamics during the initial stage (0–2 min) and end stage of sorption (1–2 h). To exclude the influence of the exposed surface area of MWCNTs on TBBPA sorption, the sorption rate was normalized with the surface area. The average sorption rate is calculated by eq 5

$$v = \frac{q_t - q_{\text{int}}}{tS_A} \tag{5}$$

where v is the average sorption rate (mg/m^2 min), q_{int} is the initial sorption amount (mg/g) at a given time (0 min or 1 h) and S_A is the surface area of MWCNTs.

2.5. Theoretical Basis. The XDLVO theory was applied to calculate the interfacial free energies of TBBPA-MWCNTs/N-MWCNTs and to explain their sorption characteristics. In this study, the interfacial free energy is basically composed of Lifshitz–van der Waals (LW) and acid–base (AB) interaction energies, as described in eq 6. Positive values of ΔG^{TOT} represent the degree of hydrophilicity repulsion, and negative values represent the degree of hydrophobicity attraction.[39]

$$\Delta G^{\text{TOT}} = \Delta G^{\text{LW}} + \Delta G^{\text{AB}} \tag{6}$$

When solid materials (1) are immersed in water (3), free energy of self-cohesion of the solid molecules is calculated by eqs 7–9

$$\Delta G_{131}^{\text{TOT}} = \Delta G_{131}^{\text{LW}} + \Delta G_{131}^{\text{AB}} \tag{7}$$

$$\Delta G_{131}^{\text{LW}} = -2(\sqrt{\gamma_1^{\text{LW}}} - \sqrt{\gamma_3^{\text{LW}}})^2 \tag{8}$$

$$\Delta G_{131}^{\text{AB}} = -4(\sqrt{\gamma_1^+\gamma_1^-} + \sqrt{\gamma_3^+\gamma_3^-} - \sqrt{\gamma_1^+\gamma_3^-} - \sqrt{\gamma_1^-\gamma_3^+}) \tag{9}$$

where $\Delta G_{131}^{\text{TOT}}$ is interfacial total free energies of self-cohesion and $\Delta G_{131}^{\text{LW}}$ and $\Delta G_{131}^{\text{AB}}$ are interfacial LW and AB free energies of self-cohesion, respectively.

When two different solid materials (1 and 2), both immersed in water (3), free energy of adhesion of the solid molecules is calculated by eq 10–12:

$$\Delta G_{132}^{\text{TOT}} = \Delta G_{132}^{\text{LW}} + \Delta G_{132}^{\text{AB}} \tag{10}$$

$$\Delta G_{132}^{\text{LW}} = -2\left(\gamma_3^{\text{LW}} + \sqrt{\gamma_1^{\text{LW}}\gamma_2^{\text{LW}}} + \sqrt{\gamma_1^{\text{LW}}\gamma_3^{\text{LW}}} - \sqrt{\gamma_2^{\text{LW}}\gamma_3^{\text{LW}}}\right) \tag{11}$$

$$\Delta G_{132}^{\text{AB}} = -2\left[\sqrt{\gamma_1^+\gamma_2^-} + \sqrt{\gamma_1^-\gamma_2^+} - \sqrt{\gamma_3^+}\left(\sqrt{\gamma_1^-} + \sqrt{\gamma_2^-} - \sqrt{\gamma_3^-}\right) - \sqrt{\gamma_3^-}\left(\sqrt{\gamma_1^+} + \sqrt{\gamma_2^+} - \sqrt{\gamma_3^+}\right)\right] \tag{12}$$

where $\Delta G_{132}^{\text{TOT}}$ is total interfacial free energies of adhesion and $\Delta G_{132}^{\text{LW}}$ and $\Delta G_{132}^{\text{AB}}$ are LW and AB interfacial free energies of adhesion, respectively. The variables γ^{LW}, γ^+, and γ^- are surface tension parameters that can be determined by contact angles measured using one apolar liquid (diiodomethane) and two different polar liquids (formamide and ultrapure water) with known surface tension parameters based on the Young equation[40] written as eq 13

$$(1 + \cos\theta)\gamma_l^{\text{TOT}} = 2\left(\sqrt{\gamma_s^{\text{LW}}\gamma_l^{\text{LW}}} + \sqrt{\gamma_s^+\gamma_l^-} + \sqrt{\gamma_s^-\gamma_l^+}\right) \tag{13}$$

where θ is the contact angle, γ^{TOT} is the total surface tension (the total surface tension is the sum of the nonpolar component γ^{LW} and the polar component γ^{AB}, as shown in eq 14; γ^+ and γ^- are an electron acceptor parameter and electron donor parameter of γ^{AB}, respectively (eq 15); and γ^{LW} represents a single electrodynamic property. The subscripts l and s in eq 13 represent liquid (i.e., three probe liquids with known surface tension parameters) and solid (i.e., the MWCNTs and TBBPA with the surface tension to be calculated), respectively.

$$\gamma^{\text{TOT}} = \gamma^{\text{LW}} + \gamma^{\text{AB}} \tag{14}$$

$$\gamma^{\text{AB}} = 2\sqrt{\gamma^+\gamma^-} \tag{15}$$

3. RESULTS AND DISCUSSION

3.1. Physicochemical Characterization of MWCNTs. The raw and modified MWCNTs were evaluated for structural integrity, surface area, and pore distribution. A comparison of SEM and TEM images of MWCNTs, O-MWCNTs, and N-MWCNTs (Supporting Information Figure S1) revealed no distinguishable changes in morphology. All samples maintained the original hollow tubular structure. The defects on the wall of modified MWCNTs likely indicate the location of grafted functional groups. The XRD powder profiles of the raw and modified MWCNTs are shown in Figure 1a. These diffractograms illustrate the characteristics of a typical MWCNT structure, which indicates a typical peak of the (002)-graphite base plane at $2\theta = 25.8°$ and a peak at approximately $2\theta = 42.8°$ assigned to the diffraction of the (100)-graphite base plane. The relatively sharp diffraction peaks demonstrate that the graphitic structures are still preserved in the carbon nanotubes.

As shown in the Raman spectra (Figure 1b), the raw and modified MWCNTs samples showed well-defined Raman bands at 1346 and 1578 cm^{-1}. The band at 1346 cm^{-1} was called the D mode, which was caused by the induction of substantial defects or disorder in the nanostructures. The position of the strong peak at 1578 cm^{-1} was due to the Raman-active vibrational E2g mode (G mode), corresponding to the structural integrity of the graphite layer.[41] Generally, the

relative intensity ID/IG was used to characterize the degree of defect in MWCNTs. The ID/IG of MWCNTs, O-MWCNTs, and N-MWCNTs was 0.8, 1.1, and 1.3, respectively. These values indicated that the original structure of MWCNTs maintained a certain degree of damage, and a certain amount of oxygen or nitrogen was introduced onto the carbon nanotube surface during the modification process. Therefore, structural defects increased, providing active reaction sites where the contaminants could be adsorbed. Almost no difference was observed when comparing the ID/IG ratios between O-MWCNTs and N-MWCNTs, indicating that the structure of O-MWCNTs was well preserved in the amino modification process.

The surface area and pore size distribution of raw and modified MWCNTs were calculated from the adsorption−desorption isotherms of N_2 at 77 K (Supporting Information Figures S2 and S3, respectively). The physical properties of the raw and modified MWCNTs are also tabulated in the Supporting Information (Table S1). The results show that as surface oxygen functional groups increased, the surface area of the MWCNTs decreased from 159.4 to 124.7 m^2/g, the total pore volume reduced from 0.94 to 0.65 cm^3/g, which indicated that the functional groups occupy a portion of the sorption sites.[42−44] Additionally, the O-MWCNTs and N-MWCNTs exhibited almost identical surface areas and pore volumes. These results support the conclusion of the obtained Raman spectrum.

The functional groups on the surfaces of the raw and modified MWCNTs are characterized by the FT-IR analysis in Figure 2. The mixed acid treatment introduces carboxyl groups

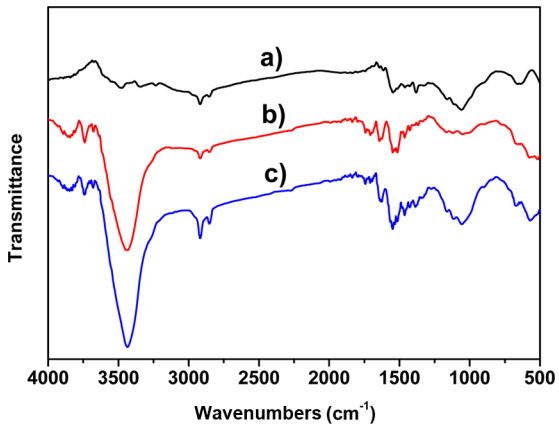

Figure 2. FT-IR spectra of (a) MWCNTs, (b) O-MWCNTs, and (c) N-MWCNTs.

onto the MWCNTs during oxidation. The intense peaks at 3438 and 1740 cm^{-1} can be attributed to the stretching vibration of the O−H groups and C═O bonds in carboxylic acid, respectively.[45] All samples were symmetrical and displayed asymmetric stretching vibration bands at 2852 and 2920 cm^{-1}.[21] Because of the $-NH_2$ stretching vibration at 3378 cm^{-1}, the peak was overlapped with the stretching vibration of ν (−OH) in the N-MWCNTs, which indicates that the EDA successfully grafted onto MWCNTs.[21,46]

The surface binding state and elemental speciation of MWCNTs were analyzed by XPS. In the wide-scan XPS survey spectra (Figure 3a), the binding energies for the C 1s, N 1s, and O 1s peaks were observed at approximately 284.5, 400.1, and 531.0 eV, respectively.[47−50] Additionally, the O 1s peak decreased and the N 1s peak appeared in the amino modified MWCNTs. Figure 3b and 3c shows the C 1s spectrum of the modified MWCNTs, which can be resolved into five sub-bands that represent the carbon in graphitic (sp^2) structures (BE ≈ 284.7 eV), aliphatic (sp^3) structures (defects on the MWCNTs structure, BE ≈ 285.3 eV), phenolic hydroxyl or carbonyl groups (BE ≈ 286.9 eV), carboxylic or ester groups (BE ≈ 288.6 eV), or the characteristic shakeup line of carbon in aromatic compounds ($\pi-\pi^*$ transition; BE ≈ 291.5 eV).[48,49,51] Figure 3d shows the deconvoluted N 1s spectra for the modified MWCNTs. The peaks at a B.E. of 399.2 and 400.1 eV (Figure 3d) are attributed to the amine nitrogen (−NH or $-NH_2$); the peaks at a BE of 400.1 and 402.8 eV are attributed to the amide nitrogen in the electron-withdrawing carbonyl group.[52−54] The carboxylic group aliphatic structures were significantly reduced on the surface of N-MWCNTs.

3.2. Effect of pH on TBBPA Sorption. The sorption behavior of TBBPA on MWCNTs was investigated at 303 K, and the pH values of the solution were adjusted to 7.0, 8.0, 9.0, and 10.0, respectively. The effects of different initial pH values on TBBPA removal were employed, and the results are given in Supporting Information Figure S4. It showed that the uptake of TBBPA sharply decreased with increasing pH values from 7.0 to 10.0, consisting with our previous study.[22,23] The amount of TBBPA adsorbed on pristine and modified MWCNTs at equilibrium decreases from 154.7 to 20.1 mg/g and from 98.5 to 4.2 mg/g, respectively. The sorption amounts of TBBPA on MWCNTs was the highest at pH = 7.0, which was mainly due to the neutral formation of TBBPA molecular. The sorption amounts of TBBPA decreased with decrease of the neutral TBBPA molecular at higher pH values. As shown in Figure 4, the zeta potential of MWCNTs and N-MWCNTs was negative and decreased with pH increasing from 4.0 to 10.0, and the pH of point of zero charge (pH_{pzc}) of N-MWCNTs was about 3.6 mV. Compared to the pristine MWCNTs, the modified MWCNTs was more hydrophilic (as presented in Supporting Information Table S2). Although these two MWCNTs owned approximate zeta potential at the same pH which range from 4.0 to 10.0, their TBBPA sorption amount varied greatly. It can be inferred that hydrophobic interaction contributed to the TBBPA sorption onto the negative charged MWCNTs in alkaline conditions. When the solution pH > pK_{a1}, the TBBPA increases in ionization and hydrophilicity, which decreases sorption because of reducing hydrophobic interactions. Ren et al. also found that the anionic form was less hydrophobic than the molecular form.[55] Fasfous et al. suggested that TBBPA was mainly in the form of a negatively charged phenoxy ion, whereas the electrostatic repulsion between the net negatively charged MWCNTs and phenoxy anions decreased the sorption at pH > pKa_1.[12] By contrast, the electrostatic repulsion compared to hydrophobic interactions was negligible.[56] Therefore, the hydrophobic interaction is considered an important mechanism for the sorption of TBBPA onto MWCNTs. The role and associated parameter values for the hydrophobic effect and van der Waals force mechanism in the sorption process are discussed and calculated in the next section.

3.3. TBBPA Sorption Kinetics. The sorption data of TBBPA over time and the pseudo-second-order kinetics model curve are presented in Supporting Information Figure S4 and Figure 5, respectively. TBBPA uptake on MWCNTs and N-MWCNTs was a rapid process. Both CNTs exhibited similar kinetics for TBBPA sorption; the reaction rate was the fastest in the 0−10 min sorption stage, contributing to 90% of the

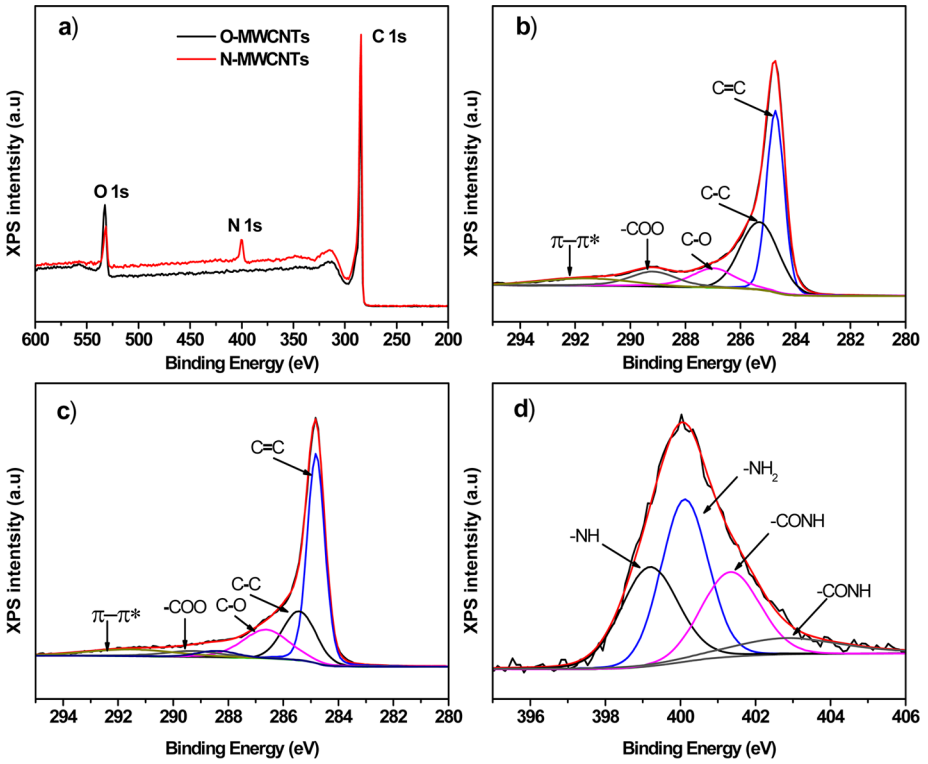

Figure 3. XPS spectra of O-MWCNTs and N-MWCNTs: (a) XPS wide-scan, (b) C 1s high-resolution spectra of O-MWCNTs, (c) C 1s, and (d) N 1s high-resolution spectra of N-MWCNTs.

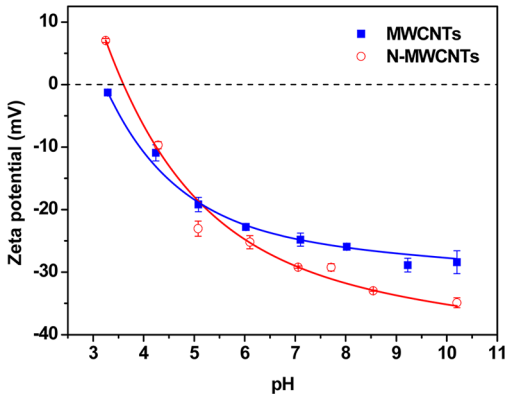

Figure 4. Zeta potentials of MWCNTs and N-MWCNTs under various pH conditions.

ultimate sorption amount. The maximum sorption capacity was achieved at approximately 20 min. Over time, the sorption capacity of TBBPA decreased. Finally, the TBBPA on MWCNTs at 1 h reached an apparent sorption equilibrium, and the sorption capacity achieved a relatively stable value. The sorption capacity during the rapid stage was slightly higher than the equilibrium sorption capacity, likely because of the large concentration gradient of pollutants between the solid–liquid phases. This gradient produced a diffusion driving force to prompt the contaminants to move quickly onto the sorbent surface.[57] In addition, the MWCNTs have a large specific surface area, and the structural defects can also serve as active sites. Over time, the solute was redistributed because of the effect of diffusion; the sorption then achieved a relatively stable state. As shown in Table 1, the calculated equilibrium sorption capacities ($q_{e,cal}$) obtained from the pseudo-second-order model were close to the experimental results ($q_{e,exp}$). This similarity indicates that the chemical interactions are involved in the sorption processes and that the sorption capacity is proportional to the number of active sites.[30]

Because the pseudo-second-order model cannot reveal a definite mechanism during the sorption process, the intraparticle diffusion model was also adopted to fit the sorption kinetics. The most important step in sorption kinetics to control the speed (rate-limiting step) is the diffusion, including external diffusion (boundary layer diffusion) and intraparticle diffusion. The intraparticle diffusion mechanism is the most important limiting factor in controlling the dynamics involved in this mechanism.[58,59] By applying the intraparticle diffusion model to the TBBPA sorption data at different pH values, whether at 2–6 min or 10 to 120 min of the sorption step, the values did not converge well and did not have straight lines that passed through the origin (Supporting Information Figure S5). Thus, the intraparticle diffusion may not be the rate-determining step.

To find the actual rate-determining step involved in the TBBPA sorption process, the sorption kinetic data was further analyzed by Boyd model. The significant property of this model is that, if the intraparticle diffusion is the sole rate-limiting step, then the linear plot of Bt against t should pass through the origin;[60,61] otherwise, it is mainly governed by external diffusion or boundary layer diffusion.[38] The plots as represented in Supporting Information Figure S6 do not pass through the origin and the data were not well correlated by the fit. This confirms that the sorption process of TBBPA onto the pristine and modified MWCNTs is controlled by external diffusion (boundary layer diffusion).

3.4. Interfacial Thermodynamic Analysis. The surface tensions, including γ^{LW}, γ^{+}, γ^{-}, γ^{AB}, and γ^{TOT}, of TBBPA and

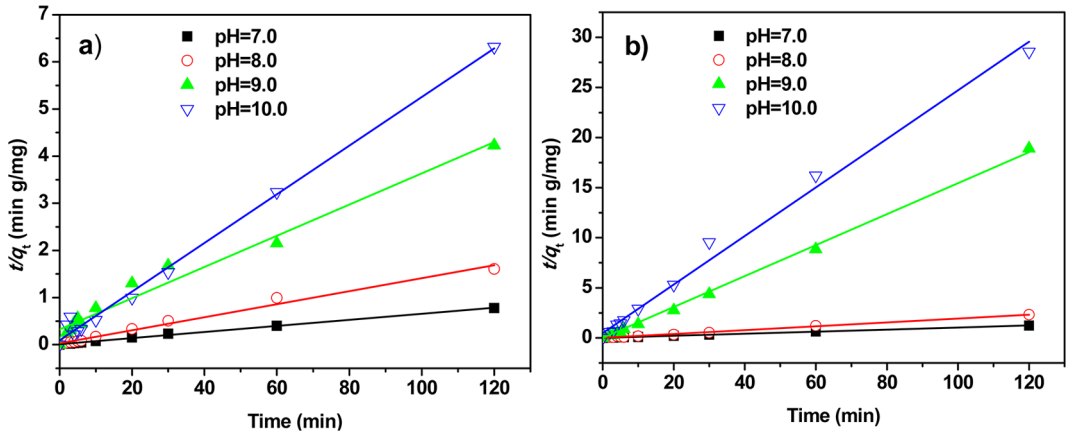

Figure 5. Pseudo-second-order model plots for TBBPA sorption on (a) MWCNTs and (b) N-MWCNTs.

Table 1. Pseudo-Second-Order Kinetics Model Parameters for TBBPA Sorption on MWCNTs and N-MWCNTs

	MWCNTs					N-MWCNTs				
pH	$q_{e,exp}$ (mg/g)	k_2 (g/mg min)	$q_{e,cal}$ (mg/g)	h (mg/g min)	R^2	$q_{e,exp}$ (mg/g)	k_2 (g/mg min)	$q_{e,cal}$ (mg/g)	h (mg/g min)	R^2
7.0	154.8	0.0036	155.0	86.49	0.998	98.5	0.010	97.5	89.29	0.999
8.0	74.8	0.0063	72.4	33.02	0.986	60.7	0.033	52.1	89.51	0.995
9.0	28.4	0.0034	30.2	3.10	0.969	9.9	~0	6.5	0	0.993
10.0	20.1	0.028	19.4	10.53	0.996	4.2	0.12	4.3	2.24	0.991

MWCNTs or N-MWCNTs at different pH levels are presented in Tables 2 and 3, respectively. The TBBPA surface tensions

Table 2. Surface Tensions (mJ/m^2) of TBBPA in Different pH Solutions

probe liquid	γ^{LW}	γ^+	γ^-	γ^{AB}	γ^{TOT}
water	43.46	0.13	3.25	1.29	44.75
pH 7.0	43.46	0.15	2.88	1.30	44.76
pH 8.0	43.46	0.13	3.26	1.29	44.75
pH 9.0	43.46	0.07	4.94	1.15	44.60
pH 10.0	43.46	0.06	5.21	1.11	44.60

(i.e., γ^+ and γ^-) were significantly influenced by pH, as shown in Table 2. In comparison to the TBBPA γ^- of 2.88 and 3.26 at pH = 7.0 and 8.0, the γ^- increased to 4.94 and 5.21 at pH = 9.0 and 10.0, respectively. Correspondingly, the γ^+ of 0.15 and 0.13 decreased to 0.07 and 0.06 at pH = 9.0 and 10.0, respectively. These alterations were due to the higher ionization of −OH of TBBPA at pH > 9.0, producing more negatively charged OH^- groups. By contrast, the surface tensions (i.e., γ^+ and γ^-) of MWCNTs and N-MWCNTs (in Table 3) changed slightly, indicating that the physical-chemical properties of MWCNTs and N-MWCNTs were stable at the different pH levels.

The interfacial free energies of adhesion for TBBPA-MWCNTs and TBBPA-N-MWCNTs implied interactions at the initial adsorption of TBBPA to MWCNTS and N-MWCNTs (Table 4). In contrast to TBBPA-N-MWCNTs, the LW interactions (i.e., ΔG_{132}^{LW}) for TBBPA-MWCNTs exhibited minimal differences; however, the AB interactions (i.e., ΔG_{132}^{AB}) for TBBPA-MWCNTs increased from −10.15 to −11.97 to −68.95 to −72.02, leading to higher average sorption rates (v) for MWCNTs than for N-MWCNTs at pH = 7.0 and 8.0 (Table 5). By contrast, the v values for MWCNTs at pH = 9.0 and 10.0 were similar to the values for N-MWCNTs, although the interfacial free energies (i.e., ΔG_{132}^{TOT}) for TBBPA-MWCNTs were greater than the values for TBBPA-N-MWCNTs. Moreover, the v values for pH = 7.0 and 8.0 were ~10 times greater than the values for pH = 9.0 and 10.0 for both MWCNTS and N-MWCNTs. These contrasts in v for different pH levels resulted from the change in the surface structure of the modified MWCNT. The oxygen- and nitrogen-containing hydrophilic functional groups on the surface modification of MWCNTs, such as hydroxy and amino, are hydrophilic groups. These groups can be combined with a number of water molecules by hydrogen bonds. This bonding may aggregate TBBPA into the interstice of MWCNTs.[26] Moreno-Castilla et al. and Lillo-Rodenas et al. found similar results for sorption onto relevant carbonaceous materials.[62,63] In addition, values of $\Delta G_{132}^{LW}/\Delta G_{132}^{AB}$ were 0.11−0.13 and 0.56−0.88 for TBBPA-MWCNTs and TBBPA-N-MWCNTs, respectively. Accordingly, the LW interactions (i.e., ΔG_{132}^{LW}) were

Table 3. Surface Tensions (mJ/m^2) of MWCNTs and N-MWCNTs in Different pH Solutions

	MWCNTs					N-MWCNTs				
probe liquid	γ^{LW}	γ^+	γ^-	γ^{AB}	γ^{TOT}	γ^{LW}	γ^+	γ^-	γ^{AB}	γ^{TOT}
water	45.76	0.73	0.52	1.23	46.99	48.74	0.35	41.34	7.60	56.34
pH 7.0	45.76	0.20	0.91	0.86	46.60	48.74	0.19	50.21	6.14	54.88
pH 8.0	45.76	0.32	0.21	0.52	46.30	48.74	0.17	51.48	5.91	54.65
pH 9.0	45.76	0.75	0.62	1.37	47.12	48.74	0.41	38.58	7.99	56.73
pH 10.0	45.76	0.76	0.65	1.40	47.16	48.74	0.46	36.67	8.24	56.98

dx.doi.org/10.1021/am505730f | ACS Appl. Mater. Interfaces 2014, 6, 20968−20977

Table 4. Interfacial Free Energies (mJ/m^2) of Adhesion for TBBPA-MWCNTs and TBBPA-N-MWCNTs in Different pH Solutions

	TBBPA-MWCNTs				TBBPA-N-MWCNTs			
probe liquid	ΔG_{132}^{TOT}	ΔG_{132}^{LW}	ΔG_{132}^{AB}	$\Delta G_{132}^{LW}/\Delta G_{132}^{AB}$	ΔG_{132}^{TOT}	ΔG_{132}^{LW}	ΔG_{132}^{AB}	$\Delta G_{132}^{LW}/\Delta G_{132}^{AB}$
water	−75.77	−8.06	−67.71	0.12	−24.91	−8.90	−16.02	0.56
pH 7.0	−77.01	−8.06	−68.95	0.12	−20.86	−8.90	−11.97	0.74
pH 8.0	−80.08	−8.06	−72.02	0.11	−19.04	−8.90	−10.15	0.88
pH 9.0	−72.42	−8.06	−64.36	0.13	−22.68	−8.90	−13.78	0.65
pH 10.0	−71.86	−8.06	−63.80	0.13	−23.40	−8.90	−14.50	0.61

Table 5. Average Sorption Rates of TBBPA-MWCNTs and TBBPA-TBBPA in Different pH Solutions

	MWCNTs		N-MWCNTs	
	$\nu_{TBBPA\text{-}MWCNTs}$ (0−2 min, mg/m^2 min)	$\nu_{TBBPA-TBBPA}$ (1−2 h, mg/m^2 min)	$\nu_{TBBPA\text{-}N\text{-}MWCNTs}$ (0−2 min, mg/m^2 min)	$\nu_{TBBPA-TBBPA}$ (1−2 h, mg/m^2 min)
pH 7.0	0.293	0.00060	0.255	0.00069
pH 8.0	0.149	0.00150	0.114	0.00027
pH 9.0	0.0247	0.00003	0.0309	0.00006
pH 10.0	0.0147	0.00003	0.0141	0.00007

not negligible, whereas hydrophobic attractive interactions (i.e., ΔG_{132}^{AB}) were dominant in TBBPA sorption onto MWCNTs.

The interfacial free energies of cohesion for TBBPA−TBBPA represented the interactions at the final stage in which the surfaces of MWCNTs/N-MWCNTs were completely covered by the adsorbed TBBPA, as presented in Table 6. In this stage,

Table 6. Interfacial Free Energies (mJ/m^2) of Cohesion for TBBPA−TBBPA in Different pH Solutions

probe liquid	ΔG_{131}^{TOT}	ΔG_{131}^{LW}	ΔG_{131}^{AB}	$\Delta G_{131}^{LW}/\Delta G_{131}^{AB}$
water	−68.34	−7.40	−60.94	0.12
pH 7.0	−69.99	−7.40	−62.59	0.12
pH 8.0	−68.28	−7.40	−60.88	0.12
pH 9.0	−61.59	−7.40	−54.19	0.14
pH 10.0	−70.30	−7.40	−62.90	0.12

the ν of MWCNTs and N-MWCNTs were both approximately zero, indicating that an sorption equilibrium of TBBPA had occurred. The interfacial free energies (i.e., ΔG_{131}^{TOT}) for TBBPA−TBBPA were from −54.19 to −62.59, similar to those of the TBBPA-MWCNT interactions. However, the ν for TBBPA-MWCNTs was significantly faster than that for TBBPA−TBBPA (approximately zero). These values likely occurred because of the diffusion driving force canceling out the attractive interactions from the interfacial free energies. The TBBPA sorption on MWCNTs achieved dynamic equilibrium.

3.5. Comparison of Adsorbent Performance with Literature Data. Different from previous studies, the maximum sorption capacities (q_{max}) of MWCNTs and N-MWCNTs used in this paper were higher, as shown in Table 6. The q_{max} of TBBPA on MWCNTs and N-MWCNTs were about 162.8 and 115.7 mg/g (obtained from Supporting Information Figure S7 and Table S3), respectively. On the contrary, the q_{max} of the MWCNTs[12] and the MWCNTs/Fe_3O_4−NH_2[13] were 66.4 and 33.7 mg/g, respectively. One of the reasons may be the solvent effect of methanol for TBBPA sorption. When methanol (5%, v/v) was added into the water solutions, the corresponding q_{max} of our MWCNTs and N-MWCNTs for TBBPA sorption at pH 7.0 were 61.3 and 42.4 mg/g at 303 K, respectively. It can be concluded that the MWCNTs was significant for TBBPA removal under water system.

Table 7. Adsorption Capacities of TBBPA on Various Adsorbents

adsorbent	pH	temperature (K)	sorption capacity (mg/g)	references
MWCNTs	7.0	303	162.8	this study
N-MWCNTs	7.0	303	115.7	this study
MWCNTs	7.0	298	64.4	12
MWCNTs/Fe_3O_4	7.0	303	22.0	13
MWCNTs/Fe_3O_4−NH_2	7.0	303	33.7	13
graphene oxide	7.0	298	115.8	22
MIEX	6.0	298	49.2	23
MNP-CTS	6.3	303	42.5	64
Fe_3O_4/GO	7.0	303	17.2	65

3.6. Potential Application of XDLVO Theory in Water Treatment. The XDLVO theory was applied to reveal the molecular interactions between adsorbents and solutes, as well as to choose an appropriate adsorbent for a given organic contaminant. On the basis of this theory, the Lifshitz−van der Waals (LW) and acid−base (AB) interactions for TBBPA-MWCNTs were successfully analyzed. It was indicated that this theory can be applied to sorption of various organic compounds. However, further work should be needed to elucidate the effects of dissolved organic matter and hardness ions, etc., on TBBPA sorption in real waters. In addition, the separation and recycling of MWCNTs should be considered.

4. CONCLUSIONS

Solution pH is an important factor affecting the sorption process of TBBPA onto MWCNTs. The uptake of TBBPA sharply decreased with increasing pH of the solution. The pH-sorption kinetics of TBBPA on MWCNTs were well described by a pseudo-second-order model, and its rate-determining steps were found to be external diffusion. During the initial sorption of TBBPA onto MWCNTS, the hydrophobic attractive interactions (i.e., interfacial AB free energies, ΔG_{132}^{AB}) for TBBPA-MWCNTs were greater than the interactions for TBBPA-N-MWCNTs, demonstrating that hydrophobic attractive interactions were dominant in TBBPA sorption onto MWCNTs. At the end of the sorption, the diffusion driving force canceled out the attractive interactions (i.e., interfacial

free energies, ΔG_{131}^{TOT}). XDLVO approaches might be necessary to reveal the interactions between sorbents and solutes.

■ ASSOCIATED CONTENT

Supporting Information

Synthesis process of O-MWCNTs and N-MWCNTs, characteristics of MWCNTs, O-MWCNTs, and N-MWCNTs (Table S1), contact angles of MWCNTs and N-MWCNTs (Table S2), isotherm parameters for TBBPA sorption on MWCNTs and N-MWCNTS (Table S3), morphology of the three MWCNTs by SEM and TEM (Figure S1), N2 adsorption−desorption isotherms and pore size distribution for the three MWCNTs (Figures S2 and S3), TBBPA sorption by MWCNTs and N-MWCNTs at different pH levels (Figure S4), intraparticle diffusion model and Boyd model plots of TBBPA sorption by MWCNTs and N-MWCNTs at different pH levels (Figures S5 and S6), and sorption isotherms of TBBPA on MWCNTs and N-MWCNTs (Figure S7). This material is available free of charge via the Internet at http://pubs.acs.org.

■ AUTHOR INFORMATION

Corresponding Authors

*Phone/fax: +86 21 65982708. E-mail: ysl@tongji.edu.cn.
*E-mail: tangyulin@tongji.edu.cn.

Notes

The authors declare no competing financial interest.

■ ACKNOWLEDGMENTS

This work was supported by National Natural Science Foundation of China (No. 21007048), Key Projects in the National Science & Technology Pillar Program during the Twelfth Five-year Plan Period (2012BAJ25B06), Twelfth Five-year Plan Period of Major Science and Technology Program for Water Pollution Control and Treatment (2012ZX07403-001) and the Collaborative Innovation Center of Advanced Technology and Equipment for Water Pollution Control and the Collaborative Innovation Center for Regional Environmental Quality.

■ REFERENCES

(1) Arnon, S.; Ronen, Z.; Yakirevich, A.; Adar, E. Evaluation of Soil Flushing Potential for Clean-up of Desert Soil Contaminated by Industrial Wastewater. *Chemosphere* **2006**, *62*, 17−25.

(2) Saint-Louis, R.; Pelletier, E. LC-ESI-MS-MS Method for the Analysis of Tetrabromobisphenol A in Sediment and Sewage Sludge. *Analyst* **2004**, *129*, 724−730.

(3) Hwang, I. K.; Kang, H. H.; Lee, I. S.; Oh, J. E. Assessment of Characteristic Distribution of PCDD/Fs and BFRs in Sludge Generated at Municipal and Industrial Wastewater Treatment Plants. *Chemosphere* **2012**, *88*, 888−894.

(4) Jiang, G. B.; Qu, G. B.; Shi, J. B.; Wang, T.; Fu, J. J.; Li, Z. N.; Wang, P.; Ruan, T. Identification of Tetrabromobisphenol A Diallyl Ether as an Emerging Neurotoxicant in Environmental Samples by Bioassay-Directed Fractionation and HPLC-APCI-MS/MS. *Environ. Sci. Technol.* **2011**, *45*, 5009−5016.

(5) Yang, S. W.; Wang, S. R.; Wu, F. C.; Yan, Z. G.; Liu, H. L. Tetrabromobisphenol A: Tissue Distribution in Fish, and Seasonal Variation in Water and Sediment of Lake Chaohu, China. *Environ. Sci. Pollut. Res.* **2012**, *19*, 4090−4096.

(6) Zhang, X. L.; Luo, X. J.; Chen, S. J.; Wu, J. P.; Mai, B. X. Spatial Distribution and Vertical Profile of Polybrominated Diphenyl Ethers, Tetrabromobisphenol A, and Decabromodiphenylethane in River Sediment from an Industrialized Region of South China. *Environ. Pollut.* **2009**, *157*, 1917−1923.

(7) Carignan, C. C.; Abdallah, M. A. E.; Wu, N.; Heiger-Bernays, W.; McClean, M. D.; Harrad, S.; Webster, T. F. Predictors of Tetrabromobisphenol-A (TBBP-A) and Hexabromocyclododecanes (HBCD) in Milk from Boston Mothers. *Environ. Sci. Technol.* **2012**, *46*, 12146−12153.

(8) Abdallah, M. A.; Harrad, S. Tetrabromobisphenol-A, Hexabromocyclododecane and Its Degradation Products in UK Human Milk: Relationship to External Exposure. *Environ. Int.* **2011**, *37*, 443−448.

(9) Thomsen, C.; Lundanes, E.; Becher, G. A Simplified Method for Determination of Tetrabromobisphenol A and Polybrominated Diphenyl Ethers in Human Plasma and Serum. *J. Sep. Sci.* **2001**, *24*, 282−290.

(10) Kawashiro, Y.; Fukata, H.; Inoue, M. O.; Kubonoya, K.; Jotaki, T.; Takigami, H.; Sakai, S. I.; Mori, C. Perinatal Exposure to Brominated Flame Retardants and Polychlorinated Biphenyls in Japan. *Endocr. J.* **2008**, *55*, 1071−1084.

(11) Kim, U. J.; Oh, J. E. Tetrabromobisphenol A and Hexabromocyclododecane Flame Retardants in Infant-Mother Paired Serum Samples, and Their Relationships with Thyroid Hormones and Environmental Factors. *Environ. Pollut.* **2014**, *184*, 193−200.

(12) Fasfous, I. I.; Radwan, E. S.; Dawoud, J. N. Kinetics, Equilibrium and Thermodynamics of the Sorption of Tetrabromobisphenol A on Multiwalled Carbon Nanotubes. *Appl. Surf. Sci.* **2010**, *256*, 7246−7252.

(13) Ji, L. Q.; Zhou, L. C.; Bai, X.; Shao, Y. M.; Zhao, G. H.; Qu, Y. Z.; Wang, C.; Li, Y. F. Facile Synthesis of Multiwall Carbon Nanotubes/Iron Oxides for Removal of Tetrabromobisphenol A and Pb (II). *J. Mater. Chem.* **2012**, *22*, 15853−15862.

(14) Zhong, Y.; Li, D.; Mao, Z.; Huang, W.; Peng, P. A.; Chen, P.; Mei, J. Kinetics of Tetrabromobisphenol A (TBBPA) Reactions with H_2SO_4, HNO_3 and HCl: Implication for Hydrometallurgy of Electronic Wastes. *J. Hazard. Mater.* **2014**, *270*, 196−201.

(15) Luo, S.; Yang, S. G.; Sun, C.; Wang, X. D. Feasibility of a Two-Stage Reduction/Subsequent Oxidation for Treating Tetrabromobisphenol A in Aqueous Solutions. *Water. Res.* **2011**, *45*, 1519−1528.

(16) Guo, Y. G.; Lou, X. Y.; Xiao, D. X.; Xu, L.; Wang, Z. H.; Liu, J. S. Sequential Reduction-Oxidation for Photocatalytic Degradation of Tetrabromobisphenol A: Kinetics and Intermediates. *J. Hazard. Mater.* **2012**, *241*, 301−306.

(17) Xu, J.; Meng, W.; Zhang, Y.; Li, L.; Guo, C. S. Photocatalytic Degradation of Tetrabromobisphenol A by Mesoporous BiOBr: Efficacy, Products and Pathway. *Appl. Catal., B* **2011**, *107*, 355−362.

(18) An, T. C.; Zu, L.; Li, G. Y.; Wan, S. G.; Mai, B. X.; Wong, P. K. One-Step Process for Debromination and Aerobic Mineralization of Tetrabromobisphenol-A by a Novel *Ochrobactrum* sp. T Isolated from an E-Waste Recycling Site. *Bioresour. Technol.* **2011**, *102*, 9148−9154.

(19) Hu, J. L.; Tong, Z. L.; Hu, Z. H.; Chen, G. W.; Chen, T. H. Adsorption of Roxarsone from Aqueous Solution by Multi-Walled Carbon Nanotubes. *J. Colloid Interface Sci.* **2012**, *377*, 355−361.

(20) Yu, F.; Ma, J.; Wu, Y. Q. Adsorption of Toluene, Ethylbenzene, and M-xylene on Multi-Walled Carbon Nanotubes with Different Oxygen Contents from Aqueous Solutions. *J. Hazard. Mater.* **2011**, *192*, 1370−1379.

(21) Hadavifar, M.; Bahramifar, N.; Younesi, H.; Li, Q. Adsorption of Mercury Ions from Synthetic and Real Wastewater Aqueous Solution by Functionalized Multi-Walled Carbon Nanotube with Both Amino and Thiolated Groups. *Chem. Eng. J.* **2014**, *237*, 217−228.

(22) Zhang, Y. H.; Tang, Y. L.; Li, S. Y.; Yu, S. L. Sorption and Removal of Tetrabromobisphenol A from Solution by Graphene Oxide. *Chem. Eng. J.* **2013**, *222*, 94−100.

(23) Tang, Y. L.; Li, S. Y.; Zhang, Y. H.; Yu, S. L.; Martikka, M. Sorption of Tetrabromobisphenol A from Solution onto Miex Resin: Batch and Column Test. *J. Taiwan. Inst. Chem. E* **2014**, *45*, 2411−2417.

(24) Yang, K.; Wu, W. H.; Jing, Q. F.; Zhu, L. Z. Aqueous Adsorption of Aniline, Phenol, and Their Substitutes by Multi-Walled Carbon Manotubes. *Environ. Sci. Technol.* **2008**, *42*, 7931−7936.

(25) Yang, K.; Wu, W. H.; Jing, Q. F.; Jiang, W.; Xing, B. S. Competitive Adsorption of Naphthalene with 2,4-Dichlorophenol and

4-Chloroaniline on Multiwalled Carbon Nanotubes. *Environ. Sci. Technol.* **2010**, *44*, 3021−3027.
(26) Pan, B.; Xing, B. S. Adsorption Mechanisms of Organic Chemicals on Carbon Nanotubes. *Environ. Sci. Technol.* **2008**, *42*, 9005−9013.
(27) Li, X. Y.; Pignatello, J. J.; Wang, Y. Q.; Xing, B. S. New Insight into Adsorption Mechanism of Ionizable Compounds on Carbon Nanotubes. *Environ. Sci. Technol.* **2013**, *47*, 8334−8341.
(28) Pan, B.; Lin, D. H.; Mashayekhi, H.; Xing, B. S. Adsorption and Hysteresis of Bisphenol A and 17 Alpha-Ethinyl Estradiol on Carbon Nanomaterials. *Environ. Sci. Technol.* **2008**, *42*, 5480−5485.
(29) Liao, Q.; Sun, J.; Gao, L. Adsorption of Chlorophenols by Multi-Walled Carbon Nanotubes Treated with HNO_3 and NH_3. *Carbon* **2008**, *46*, 553−555.
(30) Yu, Q.; Zhang, R. Q.; Deng, S. B.; Huang, J.; Yu, G. Sorption of Perfluorooctane Sulfonate and Perfluorooctanoate on Activated Carbons and Resin: Kinetic and Isotherm Study. *Water. Res.* **2009**, *43*, 1150−1158.
(31) Ojaniemi, U.; Riihimaki, M.; Manninen, M.; Pattikangas, T. Wall Function Model for Particulate Fouling Applying XDLVO Theory. *Chem. Eng. Sci.* **2012**, *84*, 57−69.
(32) Jawor, A.; Hoek, E. M. V. Removing Cadmium Ions from Water Via Nanoparticle-Enhanced Ultrafiltration. *Environ. Sci. Technol.* **2010**, *44*, 2570−2576.
(33) Brant, J. A.; Childress, A. E. Assessing Short-Range Membrane-Colloid Interactions Using Surface Energetics. *J. Membr. Sci.* **2002**, *203*, 257−273.
(34) Nishikiori, H.; Tanigaki, T.; Endo, M.; Fujii, T. Quantitative Characterization of Acidic Groups on Acid-Treated Multi-Walled Carbon Nanotubes Using 1-Aminopyrene as a Fluorescent Probe. *Carbon* **2014**, *66*, 560−566.
(35) Zang, Z. P.; Hu, Z.; Li, Z. H.; He, Q.; Chang, X. J. Synthesis, Characterization and Application of Ethylenediamine-Modified Multi-walled Carbon Nanotubes for Selective Solid-Phase Extraction and Preconcentration of Metal Ions. *J. Hazard. Mater.* **2009**, *172*, 958−963.
(36) Shen, X. E.; Shan, X. Q.; Dong, D. M.; Hua, X. Y.; Owens, G. Kinetics and Thermodynamics of Sorption of Nitroaromatic Compounds to As-Grown and Oxidized Multiwalled Carbon Nanotubes. *J. Colloid Interface Sci.* **2009**, *330*, 1−8.
(37) Boyd, G. E.; Adamson, A. W.; Meyers, L. S. The Exchange Adsorption of Ions from Aqueous Solutions by Organic Zeolites. II: Kinetics. *J. Am. Chem. Soc.* **1947**, *69*, 2836−2848.
(38) Feng, M.; You, W.; Wu, Z. S.; Chen, Q. D.; Zhan, H. B. Mildly Alkaline Preparation and Methylene Blue Adsorption Capacity of Hierarchical Flower-like Sodium Titanate. *ACS Appl. Mater. Interfaces* **2013**, *5*, 12654−12662.
(39) Li, Q. L.; Elimelech, M. Organic Fouling and Chemical Cleaning of Nanofiltration Membranes: Measurements and Mechanisms. *Environ. Sci. Technol.* **2004**, *38*, 4683−4693.
(40) van Oss, C. J.; Good, R. J. Orientation of the Water Molecules of Hydration of Human Serum Albumin. *J. Protein Chem.* **1988**, *7*, 179−183.
(41) Ying, Y. M.; Saini, R. K.; Liang, F.; Sadana, A. K.; Billups, W. E. Functionalization of Carbon Nanotubes by Free Radicals. *Org. Lett.* **2003**, *5*, 1471−1473.
(42) Yang, Y. N.; Chun, Y.; Sheng, G. Y.; Huang, M. S. pH-Dependence of Pesticide Adsorption by Wheat-Residue-Derived Black Carbon. *Langmuir* **2004**, *20*, 6736−6741.
(43) Cho, H. H.; Wepasnick, K.; Smith, B. A.; Bangash, F. K.; Fairbrother, D. H.; Ball, W. P. Sorption of Aqueous Zn [II] and Cd [II] by Multiwall Carbon Nanotubes: The Relative Roles of Oxygen-Containing Functional Groups and Graphenic Carbon. *Langmuir* **2010**, *26*, 967−981.
(44) Salam, M. A.; Burk, R. C. Thermodynamics of Pentachlorophenol Adsorption from Aqueous Solutions by Oxidized Multi-Walled Carbon Nanotubes. *Appl. Surf. Sci.* **2008**, *255*, 1975−1981.
(45) Vukovic, G. D.; Marinkovic, A. D.; Colic, M.; Ristic, M. D.; Aleksic, R.; Peric-Grujic, A. A.; Uskokovic, P. S. Removal of Cadmium from Aqueous Solutions by Oxidized and Ethylenediamine-Functionalized Multi-Walled Carbon Nanotubes. *Chem. Eng. J.* **2010**, *157*, 238−248.
(46) Vukovic, G.; Marinkovic, A.; Obradovic, M.; Radmilovic, V.; Colic, M.; Aleksic, R.; Uskokovic, P. S. Synthesis, Characterization and Cytotoxicity of Surface Amino-Functionalized Water-Dispersible Multi-Walled Carbon Nanotubes. *Appl. Surf. Sci.* **2009**, *255*, 8067−8075.
(47) Hu, H. Y.; Yu, B.; Ye, Q.; Gu, Y. S.; Zhou, F. Modification of Carbon Nanotubes with a Nanothin Polydopamine Layer and Polydimethylamino-Ethyl Methacrylate Brushes. *Carbon* **2010**, *48*, 2347−2353.
(48) Datsyuk, V.; Kalyva, M.; Papagelis, K.; Parthenios, J.; Tasis, D.; Siokou, A.; Kallitsis, I.; Galiotis, C. Chemical Oxidation of Multiwalled Carbon Nanotubes. *Carbon* **2008**, *46*, 833−840.
(49) Zhu, J. Z.; Deng, B. L.; Yang, J.; Gang, D. C. Modifying Activated Carbon with Hybrid Ligands for Enhancing Aqueous Mercury Removal. *Carbon* **2009**, *47*, 2014−2025.
(50) Valentini, L.; Macan, J.; Armentano, I.; Mengoni, F.; Kenny, J. M. Modification of Fluorinated Single-Walled Carbon Nanotubes with Aminosilane Molecules. *Carbon* **2006**, *44*, 2196−2201.
(51) Gong, H.; Kim, S. T.; Lee, J. D.; Yim, S. Simple Quantification of Surface Carboxylic Acids on Chemically Oxidized Multi-Walled Carbon Nanotubes. *Appl. Surf. Sci.* **2013**, *266*, 219−224.
(52) Kim, K. S.; Park, S. J. Influence of Amine-Grafted Multi-Walled Carbon Nanotubes on Physical and Rheological Properties of PMMA-Based Nanocomposites. *J. Solid State Chem.* **2011**, *184*, 3021−3027.
(53) Li, N.; Bai, R. B.; Liu, C. K. Enhanced and Selective Adsorption of Mercury Ions on Chitosan Beads Grafted with Polyacrylamide Via Surface-Initiated Atom Transfer Radical Polymerization. *Langmuir* **2005**, *21*, 11780−11787.
(54) Zhang, X.; Bai, R. B. Surface Electric Properties of Polypyrrole in Aqueous Solutions. *Langmuir* **2003**, *19*, 10703−10709.
(55) Ren, Y. M.; Yang, J.; Ma, W. Q.; Ma, J.; Feng, J.; Liu, X. L. The Selective Binding Character of a Molecular Imprinted Particle for Bisphenol A from Water. *Water. Res.* **2014**, *50*, 90−100.
(56) Subramani, A.; Huang, X. F.; Hoek, E. M. V. Direct Observation of Bacterial Deposition onto Clean and Organic-Fouled Polyamide Membranes. *J. Colloid Interface Sci.* **2009**, *336*, 13−20.
(57) Allen-King, R. M.; Grathwohl, P.; Ball, W. P. New Modeling Paradigms for the Sorption of Hydrophobic Organic Chemicals to Heterogeneous Carbonaceous Matter in Soils, Sediments, and Rocks. *Adv. Water. Resour.* **2002**, *25*, 985−1016.
(58) Kannan, N.; Sundaram, M. M. Kinetics and Mechanism of Removal of Methylene Blue by Adsorption on Various Carbons—A Comparative Study. *Dyes Pigments* **2001**, *51*, 25−40.
(59) Guibal, E.; McCarrick, P.; Tobin, J. M. Comparison of the Sorption of Anionic Dyes on Activated Carbon and Chitosan Derivatives from Dilute Solutions. *Sep. Sci. Technol.* **2003**, *38*, 3049−3073.
(60) Sen Gupta, S.; Bhattacharyya, K. G. Kinetics of Adsorption of Metal Ions on Inorganic Materials: A Review. *Adv. Colloid Interface Sci.* **2011**, *162*, 39−58.
(61) Wu, Z. B.; Zhong, H.; Yuan, X. Z.; Wang, H.; Wang, L. L.; Chen, X. H.; Zeng, G. M.; Wu, Y. Adsorptive Removal of Methylene Blue by Rhamnolipid-Functionalized Graphene Oxide from Wastewater. *Water. Res.* **2014**, *67*, 330−344.
(62) Moreno-Castilla, C. Adsorption of Organic Molecules from Aqueous Solutions on Carbon Materials. *Carbon* **2004**, *42*, 83−94.
(63) Lillo-Rodenas, M. A.; Cazorla-Amoros, D.; Linares-Solano, A. Behaviour of Activated Carbons with Different Pore Size Distributions and Surface Oxygen Groups for Benzene and Toluene Adsorption at Low Concentrations. *Carbon* **2005**, *43*, 1758−1767.
(64) Zhou, L. H.; Ji, L. Q.; Ma, P. C.; Shao, Y. M.; Zhang, H.; Gao, W. J.; Li, Y. F. Development of Carbon Nanotubes/$CoFe_2O_4$ Magnetic Hybrid Material for Removal of Tetrabromobisphenol A and Pb (II). *J. Hazard. Mater.* **2014**, *265*, 104−114.
(65) Ji, L. Q.; Bai, X.; Zhou, L. C.; Shi, H.; Chen, W.; Hua, Z. L. One-Pot Preparation of Graphene Oxide Magnetic Nanocomposites for the

Removal of Tetrabromobisphenol A. *Front. Environ. Sci. Eng.* **2013**, *3*, 442−450.

NOTE ADDED AFTER ASAP PUBLICATION

This paper was published on the Web on November 24, 2014, with a minor error in Figure 2. The corrected version was reposted on December 1, 2014. After the paper was reposted on December 1, 2014, additional changes were made to eq 2. The corrected version was reposted on December 10, 2014.